Pergamon

Int. J. Solids Structures Vol. 33, No. 28, pp. 4167–4193, 1996

0020-7683/96 $15.00 + .00

0020-7683(95)00268-5

A 2-D TEXTURE STUDY BASED ON A DOUBLE-SLIP MODEL OF POLYCRYSTAL PLASTICITY WITH ANALYSIS OF THIN-WALLED TUBES UNDER TORSION

ZHENGFANG QIAN* and HAN C. WU†
Department of Civil and Environmental Engineering, The University of Iowa, Iowa City, IA 52242 U.S.A.

(*Received* 1 *February* 1995; *in revised form* 1 *November* 1995)

Abstract—Elastic-plastic polycrystals are analyzed by means of a planar double-slip model. The analysis uses Taylor's assumption of uniform strain within all grains. Due to the consideration of elastic behavior, a general planar stress and strain state can be determined. Crystal hardening has been incorporated naturally into the framework of texture evolution. The concept of orientation distribution function (ODF) has been used together with its evolution equation. The overall stress components of the polycrystals are obtained analytically by the orientation (ODF) averaging. This model has then been applied to discuss the texture formation of thin-walled tubular specimens subjected to torsion. The differences between simple shear, simple (fixed-end) torsion, and pure (free-end) torsion are discussed in detail and a unified analytical solution is presented. It has been found that the theoretical axial stress of simple torsion is twice as large as that of simple shear. It has also been discovered that the development of hoop strain is directly related to the texture development during a torsion test of tube. The model also predicts the phenomenon of "tilting" of the ideal texture orientation, which has been experimentally observed. The theoretical results show very good agreement with experimental data of high purity aluminum. It may be concluded that the present model can provide a reasonable description of the torsion tests in the large strain range.

1. INTRODUCTION

Texture modeling of the microstructure of polycrystalline materials undergoing finite plastic deformation is of great technical significance in industrial working processes and it also provides important insight into the understanding of micro- and macroscopic aspects of large plastic deformation. In the experimental investigation of large plastic deformation, torsion of a thin-walled tube is an accepted test in the determination of the axial effect, which is caused by the deformation induced texture, test configuration and the material elasticity. On the other hand, the simple shearing of a material element has become a popular problem in theoretical analyses which focus on the further understanding of material behavior undergoing finite plastic deformation. The condition of simple shear is theoretically simple but is experimentally close to impossible to achieve by use of present experimental techniques. Due to lack of experimental results obtained under the simple shear condition, many authors compare their theoretical results of the simple shear problem to the experimental data obtained from the simple (fixed-end) torsion test of thin-walled tube. The simple torsion test is thus considered by many authors as an approximation test of simple shear. The two cases are, in fact, quite different and do not have the same state of stress and strain. A quantitative relation between the two cases has been derived, which provides an appropriate way to compare the results of the two cases. This point will be discussed in detail in this paper.

Texture evolution in torsion has been experimentally investigated by Jonas, Neale, Toth and their co-workers (1985, 1989, 1990, 1992), Stout and O'Rourke (1989), and Wang *et al.* (1995). Several specimen configurations have been used in the experiments. The effect of specimen geometry on the torsion test results has been investigated by Wu *et al.* (1992,

* Visiting Scholar from LNM, Institute of Mechanics, Chinese Academy of Sciences, Beijing 100080, P.R. China.
† To whom correspondence should be addressed.

1995a). It should be pointed out that torsion of solid bars and thin-walled tubes of very short gauge length (the Lindholm specimen) does provide a reasonable shear stress–strain curve, but it does not allow for the axial effect to fully develop. In order that the axial effect be investigated, Wu *et al.* (1993, 1995b) and Wang *et al.* (1995) used long, thick-walled tubular specimens. The ideal orientation of texture developed in the torsion test will be discussed in detail in this paper.

The computer simulation of texture evolution has been carried out for some simple cases of deformation by Kocks, Jonas, Asaro, Anand, Havner and their co-workers (1985, 1989, 1992, 1994). Typically, Taylor's uniform strain within all grains or relaxed constraints is assumed. The material can either be rate independent or rate dependent. The average stress and its rate in the polycrystals are then obtained by a numerical averaging procedure over the aggregate of the polycrystal. Large enough numbers of grains, such as 300, 489, or 800 grains are needed in the computation. Although computer simulations of some simple problems have been carried out by use of this method, due to its numerical nature, very little information can be extracted directly from the numerical solution that is useful for the development of phenomenological plasticity theories. Existing phenomenological plasticity theories have not adequately accounted for texture evolution. Even though the concept of plastic spin has been introduced to do the job, its evolution equation is usually not based on microscopic considerations.

An alternative approach of polycrystal plasticity, based on the concepts of orientation distribution function (ODF), its conservation equation (Clement, 1982), and ODF averaging (Rashid, 1992; Lagzdins *et al.*, 1992), but still using the general constitutive framework of continuum slip, has recently attracted the attention of researchers. Using this approach, an analysis of two-dimensional texture evolution, based on a planar double-slip model, has been conducted by Rashid (1992) and Dafalias (1993a). These authors obtained an analytical expression for the ODF function and linked the texture evolution to the distortion of the yield surface. Furthermore, the phenomenologically defined plastic spin has acquired a fundamental physical significance through the definition of a normalized average plastic spin proposed by Van Der Giessen and Van Houtte (1992) and Dafalias (1993a). This new direction for polycrystal plasticity has an advantage over the traditional one in that simple, analytical solutions may be obtained for simple benchmark problems. The analytical nature of the solutions can greatly improve the understanding of the problems at hand, and information can be extracted from the solution so that it may be used beneficially for the construction of phenomenological plasticity theories.

In the analyses of Rashid (1992) and Dafalias (1993a), by neglecting the crystal elasticity, the three stress components for the general planar stress and strain states cannot be independently determined. This drawback limits the applicability of the analyses and results in unrealistic prediction of the general two dimensional texture. Some difficulties have thus been introduced into the modeling of a tube undergoing torsion. Specifically, the axial effect and the boundary conditions of different torsion tests cannot be properly accounted for. These authors also did not incorporate crystal hardening into the evolution of texture ODF.

In the present paper, instead of rigid-perfectly-plastic grains assumed by Rashid (1992) and Dafalias (1993a), elastic-plastic polycrystals are analyzed by means of a planar double-slip model. The analysis uses Taylor's assumption of uniform strain within all grains. Due to the presence of elasticity, a general planar stress and strain state can be completely determined. Moreover, the rule of crystal hardening is incorporated naturally into the framework of texture evolution. This model has then been applied to discuss the texture formation of thin-walled tubular specimens subjected to torsion. An interesting outcome is that the theoretical axial stress of the simple torsion test (the fixed-end torsion) is exactly two times that of the simple shear. This result is independent of crystal hardening. The model also predicts the phenomenon of "tilting" in the ideal texture orientation. Analytical solutions have been obtained which clearly show the effect of crystal elasticity, boundary constraint, and texture evolution. Comparisons of theoretical results with data of torsion tests by Wu *et al.* (1993, 1995b) show that reasonable agreement has been achieved.

In Section 2, the constitutive framework for the description of finite deformation of polycrystals is given. The planar double-slip model is presented in Section 3 together with

the general solution for the general planar stress and strain problems. In Section 4, the solution for simple shear is derived with simplified assumptions of self and latent hardening. A unified solution for simple shear, simple torsion, and pure torsion is obtained in Section 5. The solution is formulated in terms of a parameter so that for different values of this parameter, the unified solution reduces to each individual case. The unified solution is derived by assuming that no hardening takes place in the crystals, i.e., the material is elastic-perfectly plastic. The differences in the conditions of stress and rate of deformation between simple shear and simple torsion and their effects are explored. In Section 6, a unified solution is given that accounts for the hardening of material. Theoretical results are then compared with experimental data obtained by Wu *et al.* (1993, 1995b) for high purity aluminum. Finally, discussion and conclusion are given in Section 7.

2. CONSTITUTIVE FRAMEWORK FOR FINITE DEFORMATION OF POLYCRYSTALS

The mechanics of crystal deformation by slip is summarized here, following Rice (1971), Hill and Rice (1972), Asaro and Rice (1977), Asaro (1983), and others. The framework of crystal slip kinematics yields (in this section, bold-faced letters denote tensors)

$$\mathbf{L} = \mathbf{D} + \mathbf{W}, \quad \mathbf{D} = \mathbf{D}^* + \mathbf{D}^{\mathrm{P}}, \quad \mathbf{W} = \boldsymbol{\omega} + \mathbf{W}^{\mathrm{P}} \tag{1a}$$

$$\mathbf{D}^{\mathrm{P}} = \sum_{\alpha} \dot{\gamma}^{(\alpha)} M^{(\alpha)}, \quad \mathbf{W}^{\mathrm{P}} = \sum_{\alpha} \dot{\gamma}^{(\alpha)} \Omega^{(\alpha)} \tag{1b}$$

with

$$M^{(\alpha)} = \tfrac{1}{2}(\mathbf{s}^{*(\alpha)} \otimes \mathbf{m}^{*(\alpha)} + \mathbf{m}^{*(\alpha)} \otimes \mathbf{s}^{*(\alpha)}), \quad \Omega^{(\alpha)} = \tfrac{1}{2}(\mathbf{s}^{*(\alpha)} \otimes \mathbf{m}^{*(\alpha)} - \mathbf{m}^{*(\alpha)} \otimes \mathbf{s}^{*(\alpha)}) \tag{1c}$$

where $\mathbf{D}$ and $\mathbf{W}$ are the symmetric and skew-symmetric parts of the velocity gradient $\mathbf{L}$; $\mathbf{D}^*$ is the rate of deformation associated with lattice elasticity; ω is the lattice spin associated with rigid rotation of the crystal; and $\mathbf{D}^{\mathrm{P}}$ and $\mathbf{W}^{\mathrm{P}}$ arise solely from the plastic slip. The αth slip system, which is defined by the unit crystallographic vectors $\mathbf{s}^{(\alpha)}$ along the slip direction and $\mathbf{m}^{(\alpha)}$ normal to the slip plane, in the reference configuration, has the shear rate of $\dot{\gamma}^{(\alpha)}$. The counterparts of these vectors, the covariant and contravariant vectors $\mathbf{s}^{*(\alpha)}$ and $\mathbf{m}^{*(\alpha)}$ in the current configuration, respectively, are approximated by orthonormal vectors when the lattice spin due to small elastic lattice distortion is neglected, compared with the large rigid lattice spin. Therefore, the resolved shear stress and its material rate, in the current configuration, can be written simply as

$$\tau^{(\alpha)} = \boldsymbol{\tau} : M^{(\alpha)} \qquad \dot{\tau}^{(\alpha)} = \boldsymbol{\tau}^{\nabla} : M^{(\alpha)} \tag{2a,b}$$

where τ, $\boldsymbol{\tau}^{\nabla}$ are the Kirchhoff stress and its lattice corotational rate, respectively; a dot over a quantity denotes the material derivative of that quantity. A rigorous framework for generalized Taylor–Schmid stress and its material rate is given by Hill and Havner (1982), and Havner (1992). As usual, the hardening law of the crystal, i.e., the evolution equation of the critical resolved shear stress $\tau_c^{(\alpha)}$, takes the following linear form of Hill (1966)

$$\dot{\tau}_c^{(\alpha)} = \sum_{\beta} h_{\alpha\beta} |\dot{\gamma}^{(\beta)}|. \tag{3}$$

Finally, the elastic behavior of the crystal is governed by Hooke's law and written as

$$\boldsymbol{\tau}^{\nabla} = \mathbf{E} : \mathbf{D}^* = \mathbf{E} : (\mathbf{D} - \mathbf{D}^{\mathrm{P}}) \qquad \boldsymbol{\tau}^{\nabla} = \dot{\boldsymbol{\tau}} - \boldsymbol{\omega} \cdot \boldsymbol{\tau} + \boldsymbol{\tau} \cdot \boldsymbol{\omega}. \tag{4a,b}$$

The elastic moduli tensor of the crystal is assumed to be isotropic for simplicity, i.e.,

$$E_{ijkl} = \lambda\delta_{ij}\delta_{kl} + \mu(\delta_{ik}\delta_{jl} + \delta_{il}\delta_{jk}) \tag{5}$$

where λ and μ are the Lamé elastic constants δ_{ij} is Kronecker's delta. A remark about this assumption will be give in Section 7.

3. PLANAR DOUBLE-SLIP IDEALIZATION

3.1. *Stress components and crystal hardening*

Instead of the rigid-plastic Taylor polycrystal considered by Rashid (1992) and Dafalias (1993a), the elastic-plastic Taylor polycrystal is considered in this investigation. In this approach, the velocity gradient tensor is known and assumed to be distributed uniformly throughout the polycrystals. In addition, the single crystal is assumed to have elastic isotropy, which is frequently assumed by researchers for simplicity, see, for instance, Nemat-Nasser and Obata (1986). This assumption was also made by Lin (1964) in his modification of Taylor's model in the case of small deformation. The planar double-slip here is in the sense of the effective double-slip idealization of Rashid (1992) which is consistent with Asaro (1983) and Havner (1992). Following Rashid (1992), for the planar-double slip model, (1) reduces to

$$\dot{\gamma}^{(1)} = \frac{2}{\sin 4\alpha}(D^P_{11}\cos 2\beta_2 - D^P_{12}\sin 2\beta_2), \quad \beta_2 = \theta - \alpha \tag{6a}$$

$$\dot{\gamma}^{(2)} = \frac{2}{\sin 4\alpha}(D^P_{12}\sin 2\beta_1 - D^P_{11}\cos 2\beta_1), \quad \beta_1 = \theta + \alpha \tag{6b}$$

where the angle 2α is the separation angle between the two slip systems, and the angle θ defines the current orientation of the slip-system pair, as shown in Fig. 1. It is noted that the present configuration of double-slip is slightly different than Rashid's for the convenience of a tubular specimen under torsion. The angles β_1 and β_2 are the current orientations of the individual slip systems. By use of (1c), (2a) reduces to

$$\tfrac{1}{2}(\tau_{11} - \tau_{22}) = \frac{1}{\sin 4\alpha}(\tau^{(1)}\cos 2\beta_2 - \tau^{(2)}\cos 2\beta_1) \tag{7a}$$

$$\tau_{12} = \frac{1}{\sin 4\alpha}(\tau^{(2)}\sin 2\beta_1 - \tau^{(1)}\sin 2\beta_2). \tag{7b}$$

The three components of local stress, τ_{11}, τ_{22}, τ_{12}, are not determined by the above two

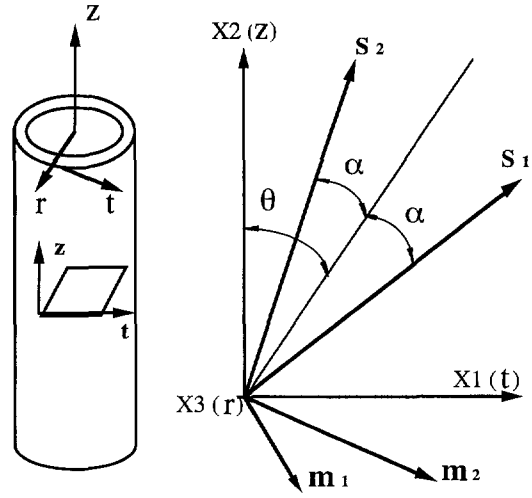

Fig. 1. The planar double-slip systems and the coordinate axes.

equations. Instead of determining the two quantities $(\tau_{11}-\tau_{22})$ and τ_{12} as in Rashid (1992) and Dafalias (1993a), a third equation is added by considering the elastic behavior. Due to the assumption of plastic incompressibility, i.e., $D^P_{kk}=0$, (4a) reduces to

$$\tau^{\nabla}_{kk}=(3\lambda+2\mu)D_{kk}. \tag{8}$$

This is the additional equation that is needed to determine the stress components. In order to integrate this equation, the following relation for the planar double-slip system is used:

$$M^{(\alpha)}_{11}+M^{(\alpha)}_{22}=0 \quad \text{and} \quad D^P_{11}+D^P_{22}=0, \quad (\alpha=1,2) \tag{9}$$

so that $D^P_{33}=0$, and in the case of planar stress state, the 33 component of (4a) leads to

$$\tau_{33}=\tau^{\nabla}_{33}=0, \quad D^P_{33}=0, \quad D_{33}=-\frac{\lambda}{\lambda+2\mu}(D_{11}+D_{22}). \tag{10a}$$

On the other hand, in the case of plane strain, the relations are

$$D_{33}=D^P_{33}=0, \quad \tau^{\nabla}_{33}=\dot{\tau}_{33}=\lambda(D_{11}+D_{22}) \tag{10b}$$

so that, from (4b), for both cases

$$\tau^{\nabla}_{11}+\tau^{\nabla}_{22}=\dot{\tau}_{11}+\dot{\tau}_{22}=2E_1(D_{11}+D_{22}) \tag{11a}$$

with

$$E_1=\begin{cases}\dfrac{3\lambda+2\mu}{\lambda+2\mu}\mu & \text{for plane stress}\\ \lambda+\mu & \text{for plane strain}\end{cases}. \tag{11b}$$

This equation may then be integrated to yield

$$\tau_{11}+\tau_{22}=2E_1\int_0^t(D_{11}+D_{22})\,\mathrm{d}t. \tag{12}$$

The solution of (7a, b) and (12) is

$$\tau_{11}=E_1\int_0^t(D_{11}+D_{22})\,\mathrm{d}t+\frac{1}{\sin 4\alpha}(\tau^{(1)}\cos 2\beta_2-\tau^{(2)}\cos 2\beta_1) \tag{13a}$$

$$\tau_{22}=E_1\int_0^t(D_{11}+D_{22})\,\mathrm{d}t-\frac{1}{\sin 4\alpha}(\tau^{(1)}\cos 2\beta_2-\tau^{(2)}\cos 2\beta_1) \tag{13b}$$

$$\tau_{12}=\frac{1}{\sin 4\alpha}(\tau^{(2)}\sin 2\beta_1-\tau^{(1)}\sin 2\beta_2). \tag{13c}$$

Similarly, from (2b), expressions for $(\tau^{\nabla}_{11}-\tau^{\nabla}_{22})$ and τ^{∇}_{12} can be obtained. These expressions and (11a) may be solved together to find

$$\tau^{\nabla}_{11}=E_1(D_{11}+D_{22})+\frac{1}{\sin 4\alpha}(\dot{\tau}^{(1)}\cos 2\beta_2-\dot{\tau}^{(2)}\cos 2\beta_1) \tag{14a}$$

$$\tau^{\nabla}_{22}=E_1(D_{11}+D_{22})-\frac{1}{\sin 4\alpha}(\dot{\tau}^{(1)}\cos 2\beta_2-\dot{\tau}^{(2)}\cos 2\beta_1) \tag{14b}$$

$$\tau_{12}^{\nabla} = \frac{1}{\sin 4\alpha}(\dot{\tau}^{(2)} \sin 2\beta_1 - \dot{\tau}^{(1)} \sin 2\beta_2). \tag{14c}$$

Therefore, the three co-rational stress rates τ_{11}^{∇}, τ_{22}^{∇}, τ_{12}^{∇} are determined by (14) when the material time derivatives, $\dot{\tau}^{(1)}$ and $\dot{\tau}^{(2)}$, of the double slip system are given. Now, from (4a), the plastic strain rate D_{ij}^{P} may be expressed in terms of D_{ij} τ_{ij}^{∇}, and the Lamé constants, λ and μ. The expressions are then substituted into (6) to obtain

$$\dot{\gamma}^{(1)} = \frac{2}{\sin 4\alpha}\left(\frac{\tau_{12}^{\nabla}}{2\mu}\sin 2\beta_2 - \frac{\tau_{11}^{\nabla}}{2\mu}\cos 2\beta_2 + D'\cos 2\beta_2 - D_{12}\sin 2\beta_2\right) \tag{15a}$$

$$\dot{\gamma}^{(2)} = \frac{2}{\sin 4\alpha}\left(\frac{\tau_{11}^{\nabla}}{2\mu}\cos 2\beta_1 - \frac{\tau_{12}^{\nabla}}{2\mu}\sin 2\beta_1 - D'\cos 2\beta_1 + D_{12}\sin 2\beta_1\right) \tag{15b}$$

where

$$D' = \begin{cases} D_{11} + \dfrac{\lambda}{\lambda+2\mu}(D_{11}+D_{22}) & \text{for plane stress} \\ D_{11} + \dfrac{\lambda}{2\mu}(D_{11}+D_{22}) & \text{for plane strain} \end{cases}. \tag{15c}$$

The connection between slip shear rates $\dot{\gamma}^{(\alpha)}$ and rates $\dot{\tau}^{(\alpha)}$ of the Schmid resolved shear stresses, in general, can be realized through the hardening law of the crystal. In two dimensional polycrystals, double slip systems are always assumed to be activated simultaneously during loading. Equations in (6) shows that the slip shear rates $\dot{\gamma}^{(1)}$ and $\dot{\gamma}^{(2)}$ are usually not equal to zero at the same time for any orientation θ, except when both D_{12}^{P} and D_{11}^{P} are equal to zero. In the latter case, (15) reduces to Hooke's law (given by (4)) by setting $\dot{\gamma}^{(1)} = \dot{\gamma}^{(2)} = 0$. This case, in fact, describes the elastic loading and/or unloading. In the case of monotonic loading, the crystal hardens according to the following rule

$$\dot{\tau}^{(\alpha)} = \dot{\tau}_c^{(\alpha)} \operatorname{sign}(\dot{\gamma}^{(\alpha)}), \quad \tau^{(\alpha)} = [\tau_0^{(\alpha)} + \int \dot{\tau}_c^{(\alpha)}\, dt] \operatorname{sign}(\dot{\gamma}^{(\alpha)}), \quad (\alpha = 1, 2). \tag{16}$$

The notation sign $(\dot{\gamma}^{(\alpha)})$ is used to indicate forward (positive) or reverse (negative) slip. When both slip shear rates $\dot{\gamma}^{(1)}$ and $\dot{\gamma}^{(2)}$ are positive, then from (5) and (16), the hardening rule is written as

$$\dot{\tau}^{(1)} = h_{11}\dot{\gamma}^{(1)} + h_{12}\dot{\gamma}^{(2)} \tag{17a}$$

$$\tau^{(2)} = h_{21}\dot{\gamma}^{(1)} + h_{22}\dot{\gamma}^{(2)} \tag{17b}$$

where h_{11}, h_{22} are the self-hardening moduli, and h_{12}, h_{21} the latent hardening moduli. The latent hardening of crystals in double-slip was discussed by Havner and Salpekar (1982, 1983). A comprehensive study of this subject is also given by Havner (1992). Combining (14) with (17) and then with (15), the resulting equations can be solved for the following explicit expressions of lattice corotational rates of stress components

$$\frac{\tau_{11}^{\nabla}}{\mu} = \frac{\eta A + (a_{12}B - b_{12}A) + \eta E_1(\eta - b_{12})(D_{11}+D_{22})}{\mu[(\eta - a_{22})(\eta - b_{12}) - a_{12}b_{22}]} \tag{18a}$$

$$\frac{\tau_{12}^{\nabla}}{\mu} = \frac{\eta B + (b_{22}A - a_{22}B) + \eta E_1 b_{22}(D_{11}+D_{22})}{\mu[(\eta - a_{22})(\eta - b_{12}) - a_{12}b_{22}]} \tag{18b}$$

$$\frac{\tau_{22}^{\nabla}}{\mu} = 2\frac{E_1}{\mu}(D_{11}+D_{22}) - \frac{\tau_{11}^{\nabla}}{\mu} \tag{18c}$$

where

$$A = (h_{11}\cos 2\beta_2 - h_{21}\cos 2\beta_1)(D'\cos 2\beta_2 - D_{12}\sin 2\beta_2) - (h_{12}\cos 2\beta_2 - h_{22}\cos 2\beta_1)(D'\cos 2\beta_1 - D_{12}\sin 2\beta_1) \tag{18d}$$

$$B = (h_{21}\sin 2\beta_1 - h_{11}\sin 2\beta_2)(D'\cos 2\beta_2 - D_{12}\sin 2\beta_2) - (h_{22}\sin 2\beta_1 - h_{12}\sin 2\beta_2)(D'\cos 2\beta_1 - D_{12}\sin 2\beta_1) \tag{18e}$$

$$a_{12} = \frac{1}{2\mu}[\sin 2\beta_2(h_{11}\cos 2\beta_2 - h_{21}\cos 2\beta_1) - \sin 2\beta_1(h_{12}\cos 2\beta_2 - h_{22}\cos 2\beta_1)] \tag{18f}$$

$$a_{22} = \frac{1}{2\mu}[\cos 2\beta_1(h_{12}\cos 2\beta_2 - h_{22}\cos 2\beta_1) - \cos 2\beta_2(h_{11}\cos 2\beta_2 - h_{21}\cos 2\beta_1)] \tag{18g}$$

$$b_{12} = \frac{1}{2\mu}[\sin 2\beta_2(h_{21}\sin 2\beta_1 - h_{11}\sin 2\beta_2) - \sin 2\beta_1(h_{22}\sin 2\beta_1 - h_{12}\sin 2\beta_2)] \tag{18h}$$

$$b_{22} = \frac{1}{2\mu}[\cos 2\beta_1(h_{22}\sin 2\beta_1 - h_{12}\sin 2\beta_2) - \cos 2\beta_2(h_{21}\sin 2\beta_1 - h_{11}\sin 2\beta_2)] \tag{18i}$$

$$\eta = \tfrac{1}{2}(\sin 4\alpha)^2. \tag{18j}$$

When one of the slip rates, or both, are negative, similar expressions can be obtained by simply replacing the signs of hardening moduli in the above equations according to the signs of slip shear rates.

3.2. *Orientation averaging and texture evolution*

The orientation of the slip system is specified by the angle θ, which is related to the lattice spin ω_{12}, following Rashid (1992), by

$$\dot{\theta} = -\boldsymbol{\omega}_{12} = \tfrac{1}{2}(\dot{\gamma}^{(1)} + \dot{\gamma}^{(2)}) - \mathbf{W}_{12}. \tag{19a}$$

Combining (15) with (19a), the rate of change of θ is found to be

$$\dot{\theta} = \frac{1}{\sin 4\alpha}\left[\frac{\tau_{11}^{\nabla}}{2\mu}(\cos 2\beta_1 - \cos 2\beta_2) + \frac{\tau_{12}^{\nabla}}{2\mu}(\sin 2\beta_2 - \sin 2\beta_1) + D_{12}(\sin 2\beta_1 - \sin 2\beta_2) + D'(\cos 2\beta_2 - \cos 2\beta_1)\right] - W_{12}. \tag{19b}$$

Therefore, by substituting (18) into (15), the slip rates are determined, and from (19) the lattice spin can be found. On the other hand, the local stresses τ_{11}, τ_{22}, τ_{12} are obtained by first finding $\tau^{(\alpha)}$ from (16), (17), (15), (18) and then using (13). Finally, the overall stress components of the polycrystals are obtained through the orientation averaging approach discussed by Rashid (1992) and Lagzdins *et al.* (1992), i.e.,

$$\sigma_{11}(t) = \frac{1}{\pi}\int_{-\pi/2}^{\pi/2} \tau_{11}(\theta, t) f(\theta, t)\, \mathrm{d}\theta \tag{20a}$$

$$\sigma_{22}(t) = \frac{1}{\pi}\int_{-\pi/2}^{\pi/2} \tau_{22}(\theta, t) f(\theta, t)\, \mathrm{d}\theta \tag{20b}$$

$$\sigma_{12}(t) = \frac{1}{\pi}\int_{-\pi/2}^{\pi/2} \tau_{12}(\theta, t) f(\theta, t)\, \mathrm{d}\theta \tag{20c}$$

where $f(\theta, t)$ is the orientation distribution function (ODF) which will change with respect to deformation history and loading path. The evolution equation of the ODF is given in Clement (1982) and Rashid (1992) as

$$\frac{\partial f}{\partial t} + \frac{\partial(f\dot{\theta})}{\partial \theta} = 0, \quad \text{with} \quad \frac{1}{\pi}\int_{-\pi/2}^{\pi/2} f(\theta, t)\, \mathrm{d}\theta = 1. \tag{21}$$

The lattice spin ω_{12} depends only on angle θ in several studies of two-dimensional texture evolution, such as Rashid (1992), Dafalias (1993a), and Van Der Giessen (1989). Even though it may depend on the loading history in the more general case, the following simplified form is assumed as an approximation for the simple loading history considered in this investigation:

$$\dot{\theta} = -\omega_{12} = R(\theta) \tag{22}$$

where $R(\theta)$ is a function of orientation θ. Using (22), the evolution equation for the case of two-dimensional texture is

$$\frac{\partial f}{\partial t} + R(\theta)\frac{\partial f}{\partial \theta} = -f\frac{\mathrm{d}R(\theta)}{\mathrm{d}\theta} \tag{23}$$

which is now solved by the method of characteristics. The equations along the characteristics are

$$\frac{\mathrm{d}t}{1} = \frac{\mathrm{d}\theta}{R(\theta)} = -\frac{\mathrm{d}f/f}{\mathrm{d}R(\theta)/\mathrm{d}\theta}. \tag{24}$$

These equations may be integrated to yield

$$\mathrm{d}t = \frac{\mathrm{d}\theta}{R(\theta)} \quad \text{and} \quad t = \int_{\theta_0}^{\theta} \frac{\mathrm{d}\theta}{R(\theta)} \tag{25}$$

and

$$\frac{\mathrm{d}f}{f} = -\frac{\mathrm{d}R(\theta)}{R(\theta)} \quad \text{and} \quad \log\left(\frac{f}{f_0}\right) = -\log\left(\frac{R(\theta)}{R(\theta_0)}\right) \tag{26}$$

in which $f_0 = f(\theta, t = 0) = 1$ is the initial condition. At the beginning, the ODF has the value of one because of the assumption of random grain distribution. The general solution is then written as

$$f(\theta, t) = \frac{R(\theta_0)}{R(\theta)}. \tag{27}$$

It is noted that the parameter θ_0 on the characteristic line depends on both time t and

orientation angle θ according to (25). Therefore, it is not a constant. The general solution was also obtained by Prantil *et al.* (1993) using a different derivation.

In summary, the governing equations for the textured polycrystals under general planar stress or strain states have been derived in this section in a closed form. Three independent stress components are determined completely, and the information of crystal hardening has also been naturally incorporated into the texture evolution equations. Application to some special states of stress and strain by use of these equations is presented in the remaining part of this paper.

4. SIMPLE SHEAR

This section is focused on simple shear because of its importance and simplicity. Simple shear is the simplest test problem for any theory of finite deformation. In order to bring out special features of this model, in particular the effect of material hardening on ideal orientation, a simple case of strain-hardening is considered, so that

$$h_{11} = h_{22} = h(t), \quad h_{12} = h_{21} = qh(t). \tag{28}$$

where the ratio q of latent hardening is a constant. The equations of this section pertain to the case of positive slip rates. The case of non-positive slip rates will be addressed in Section 6. In the case of simple shear, the rate of deformation and material spin are

$$D_{11} = D_{22} = D' = 0, \quad D_{12} = D_{21} = W_{12} = -W_{21} = \text{constant}. \tag{29}$$

By applying condition (29) in (12) and (20), the stress of the polycrystals must satisfy the following relation in simple shear

$$\sigma_{11} + \sigma_{22} = 0 \quad \text{or} \quad \sigma_{22} = -\sigma_{11} \neq 0. \tag{30}$$

Using (28) and (29), (18) becomes

$$\frac{\tau^{\nabla}_{11}}{\mu} = -\frac{\tau^{\nabla}_{22}}{\mu} = \frac{\dfrac{h}{\mu} D_{12}(q - \cos 4\alpha) \sin 4\theta}{\eta + \dfrac{h}{\mu}(1 - q\cos 4\alpha) + \dfrac{1}{2}\left(\dfrac{h}{\mu}\right)^2 (1 - q^2)} \tag{31a}$$

$$\frac{\tau^{\nabla}_{12}}{\mu} = \frac{\dfrac{h}{\mu} D_{12}\left[(1 - q\cos 4\alpha) + \dfrac{h}{\mu}(1 - q^2) + (q - \cos 4\alpha)\cos 4\theta\right]}{\eta + \dfrac{h}{\mu}(1 - q\cos 4\alpha) + \dfrac{1}{2}\left(\dfrac{h}{\mu}\right)^2 (1 - q^2)}. \tag{31b}$$

The shear rates of the double slip system may then be obtained from (15a) and (15b), using (29), (31a), and (31b). The results are

$$\dot{\gamma}^{(1)} = \frac{2D_{12}}{\sin 4\alpha}[(1 - H)\sin 2\alpha \cos\theta - (1 - Q)\cos 2\alpha \sin 2\theta] \tag{32a}$$

$$\dot{\gamma}^{(2)} = \frac{2D_{12}}{\sin 4\alpha}[(1 - H)\sin 2\alpha \cos 2\theta + (1 - Q)\cos 2\alpha \sin 2\theta] \tag{32b}$$

with two dimensionless hardening parameters

$$H = \frac{\frac{h}{2\mu}(1+q)\left[1 \quad \cos 4\alpha + \frac{h}{\mu}(1-q)\right]}{\eta + \frac{h}{\mu}(1-q\cos 4\alpha) + \frac{1}{2}\left(\frac{h}{\mu}\right)^2(1-q^2)} \tag{32c}$$

and

$$Q = \frac{\frac{h}{2\mu}(1-q)\left[1+\cos 4\alpha + \frac{h}{\mu}(1+q)\right]}{\eta + \frac{h}{\mu}(1-q\cos 4\alpha) + \frac{1}{2}\left(\frac{h}{\mu}\right)^2(1-q^2)} \tag{32d}$$

where $H = h = 0$ corresponds to the case of no hardening and $Q = 0$ corresponds to the case of latent hardening equal to self hardening with $q = 1$.

By substituting (32) into (19a), the rate of θ is found to be

$$R(\theta) = \dot{\theta} = \frac{D_{12}}{\cos 2\psi}(\cos 2\theta - \cos 2\psi), \quad \cos 2\psi = \frac{\cos 2\alpha}{1-H}. \tag{33}$$

The equilibrium value θ_s of the angle θ, i.e., the ideal orientation of the texture, can be obtained by setting $\mathrm{d}\theta/\mathrm{d}t = 0$ in (33) and has been determined to be

$$0 \leqslant \theta_s = \psi \leqslant \alpha, \quad H \geqslant 0. \tag{34}$$

It is seen from (33) and (34) that crystal hardening influences texture evolution and the ideal orientation of texture through parameter H, and that the ideal orientation θ_s depends on the material characteristic angle α of the equivalent double-slip system, the normalized self hardening h/μ, and the latent hardening ratio q. Note that H is of the order h/μ in magnitude, which is much less than unity. Therefore, the hardening of materials, in the case of simple shear, does not have a significant influence on the ideal orientation and ODF evolution. However, the material hardening is important when it is combined with the effect of boundary constraints, such as tubular specimen under torsion. This situation will be reported in Section 6.

The explicit expression of ODF for the case of simple shear will now be derived from (33) and (25). This procedure will be used again in later sections. The resulting equation is

$$(2D_{12}t)\tan(2\psi) = \int_{\theta_0}^{\theta} \frac{2\sin 2\psi \,\mathrm{d}\theta}{\cos(2\theta) - \cos(2\psi)} = \int_{\theta_0}^{\theta}\left[\frac{\cos(\psi-\theta)}{\sin(\psi-\theta)} + \frac{\cos(\psi+\theta)}{\sin(\psi+\theta)}\right]\mathrm{d}\theta \tag{35}$$

or

$$\frac{\sin(\psi+\theta)}{\sin(\psi-\theta)}\left(\frac{\tan\psi - \tan\theta_0}{\tan\psi + \tan\theta_0}\right) = \mathrm{e}^{\Gamma t}, \quad \Gamma = 2D_{12}\tan(2\psi). \tag{36}$$

The parameter θ_0 can be determined from the above equation as

$$\tan\theta_0 = \tan\psi \frac{\sin(\psi+\theta) - \sin(\psi-\theta)\,\mathrm{e}^{\Gamma t}}{\sin(\psi+\theta) + \sin(\psi+\theta)\,\mathrm{e}^{\Gamma t}}, \quad \cos 2\theta_0 = \frac{1-\tan^2\theta_0}{1+\tan^2\theta_0}. \tag{37}$$

Finally, the expression of ODF is found from (27), (33) and (37) as

$$f(\theta, t) = \frac{\cos 2\theta_0 - \cos 2\psi}{\cos 2\theta - \cos 2\psi} = \frac{\sin^2 2\psi}{a + b\sin 2\theta + c\cos 2\theta}$$

$$= \frac{e^{\Gamma t}\sin^2 2\psi}{[\sin(\psi+\theta) + e^{\Gamma t}\sin(\psi-\theta)]^2 - 4e^{\Gamma t}\sin(\psi+\theta)\sin(\psi-\theta)\sin^2\psi} \tag{38a}$$

where

$$\begin{cases} a = \sin^2 2\psi + 2\sinh^2(\frac{1}{2}\Gamma t) \\ b = -2\sinh(\frac{1}{2}\Gamma t)\cosh(\frac{1}{2}\Gamma t)\sin 2\psi. \\ c = -2\sinh^2(\frac{1}{2}\Gamma t)\cos 2\psi \end{cases} \tag{38b}$$

The ODF expression in (38) is the same as the one derived by Rashid (1992) and Dafalias (1993a). However, the present method of derivation is different and more straightforward.

5. UNIFIED SOLUTION OF SIMPLE SHEAR, SIMPLE TORSION AND PURE TORSION FOR ELASTIC-PERFECTLY-PLASTIC MATERIAL

The goal of this section is to investigate the similarity and differences between simple shear and torsion of thin-walled tubes due to different deformation states and geometries. For simplicity, the effect of material hardening has been removed by considering the special case of no hardening, i.e., elastic-perfectly-plastic material. A unified solution is presented to clarify some of the confusion that has arisen from the attempt to use the simple shear state to model torsion of a thin-walled tube with fixed-end. Some of these problems have been addressed by White (1992) by use of the finite element method.

The coordinate system, shown in Fig. 1, is used to facilitate the investigation of a tubular specimen under torsion. The hoop (shear) direction is denoted by X_1 or t; the axial direction is denoted by X_2 or z; and the radial direction is denoted by X_3 or r. Then, the relevant components of $\mathbf{D}$, $\mathbf{W}$, and σ are

$$D_{11} = D_{tt}, \quad D_{22} = D_{zz}, \quad D_{33} = D_{rr}, \quad D_{12} = D_{tz}, \quad W_{12} = W_{tz};$$

$$\sigma_{11} = \sigma_{tt}, \quad \sigma_{22} = \sigma_{zz}, \quad \sigma_{33} = \sigma_{rr}, \quad \sigma_{12} = \sigma_{tz}.$$

The conditions required by the specific geometry of the problem for simple shear, simple torsion (torsion of a thin-walled tube with fixed-ends), and pure torsion (torsion of a thin-walled tube with free-ends), are now summarized as:
Simple shear

$$D_{zz} = D_{tt} = D_{rr} = 0, \quad D_{tz} = W_{tz} = \text{const.}; \quad \sigma_{tt} = -\sigma_{zz}; \quad D' = 0. \tag{39}$$

Simple torsion

$$D_{zz} = 0, \quad D_{tt} \neq 0, \quad D_{tz} = W_{tz} = \text{const.}; \quad \sigma_{tt} = 0, \quad \sigma_{zz} \neq 0, \quad \sigma_{rr} = 0; \quad D' = 2\frac{\lambda+\mu}{\lambda+2\mu}D_{tt}. \tag{40}$$

Pure torsion

$$D_{zz} = -D_{tt}, \quad D_{rr} \approx 0, \quad D_{tz} = W_{tz} = \text{const.}; \quad \sigma_{tt} = \sigma_{zz} = \sigma_{rr} = 0; \quad D' = D_{tt}. \tag{41}$$

The differences among the three cases are clear from (39), (40) and (41). In the case of simple shear, eqns (39), (12) and (20) lead to the results that the hoop stress, $\boldsymbol{\sigma}_{tt}$, be equal to the negative of the axial stress, $\boldsymbol{\sigma}_{zz}$, and that the hoop strain rate D_{tt} be zero. However, in the torsion test of a tubular specimen, the hoop stress, $\boldsymbol{\sigma}_{tt}$, is zero due to symmetry and

force equilibrium, and the hoop strain is allowed to develop due to texture formation. Therefore, the stress and strain states of simple shear and simple torsion are quite different. In the case of simple torsion, (10a) reduce to $D_{rr} = -(\nu/1-\nu)D_{tt}$, where ν is Poisson's ratio. Thus, $D_{rr} \neq -D_{tt}$ in general. However, in this case, the change in the diameter and the wall-thickness is so small that it is difficult to measure with the available experimental techniques. Nevertheless, D_{tt} does have an important effect in the solution of simple torsion and this will be demonstrated later. Wu *et al.* (1993, 1995b) found experimentally that the hoop strain is approximately equal to the axial strain in magnitude in the case of pure torsion. Due to the assumption of plastic incompressibility of the material, the change in wall-thickness during pure torsion is negligible. The relation of $D_{tt} = -D_{zz}$, $D_{rr} = 0$ for pure torsion from (12), (20) and (10a) is thus seen to be reasonable.

Using a procedure similar to that used in the derivation of (32) and the conditions of (39), (40) and (41), the slip shear rates are obtained and written in a unified form for all three cases as

$$\dot{\gamma}^{(1)} = \frac{2}{\sin 4\alpha}(\zeta D_{tt}\cos 2\beta_2 - D_{tz}\sin 2\beta_2) \tag{42a}$$

$$\dot{\gamma}^{(2)} = \frac{2}{\sin 4\alpha}(-\zeta D_{tt}\cos 2\beta_1 + D_{tz}\sin 2\beta_1) \tag{42b}$$

and the rate of change of ideal orientation is

$$\dot{\theta} = \frac{D_{tz}}{\cos 2\psi}[\cos(2\theta+2\phi) - \cos 2\psi], \quad \cos 2\psi = \cos 2\alpha \cos 2\phi, \quad \tan 2\phi = -\zeta\frac{D_{tt}}{D_{tz}} \tag{43a}$$

where

$$\zeta = \begin{cases} 0 & \text{for simple shear} \\ 0.5 & \text{for simple torsion.} \\ 1.0 & \text{for pure torsion} \end{cases} \tag{43b}$$

Note that (43a) can be obtained by replacing θ by $\theta+\phi$ in (33) and the expression of ODF is obtained by replacing θ in (38a) by $\theta+\phi$, but with different expressions of a, b, and c which are to be given later in (46f). The characteristic angles ψ and ϕ, defined in (43a), are directly related to the development of hoop strain rate D_{tt} due to texture formation and are also dependent on boundary constraint conditions of the torsion test. It is seen from (43a) that the ideal orientation is in the orientation $(\psi-\phi)$ for both cases of torsion, but it is in the orientation α for simple shear. In the latter case, $\phi = 0$ and $\psi = \alpha$, which may also be obtained by letting $H = 0$ in (33). More discussions about the ideal orientation will be given later together with numerical examples.

For elastic-perfectly plastic material, the resolved shear stresses, (16), for the two slip systems are given by

$$\tau^{(1)} = \tau_0 \operatorname{sign}(\dot{\gamma}^{(1)}), \quad \tau^{(2)} = \tau_0 \operatorname{sign}(\dot{\gamma}^{(2)}) \tag{44}$$

where the critical resolved shear stress is constant, i.e., $\tau_0^{(1)} = \tau_0^{(2)} = \tau_0$. Therefore, (13a), (13b) and (13c) are simplified and become

$$\tau_{zz} = E_1 \int_0^t (D_{tt} + D_{zz})\,\mathrm{d}t - \frac{\tau_0}{\sin 4\alpha}[\cos 2\beta_2 \operatorname{sign}(\dot{\gamma}^{(1)}) - \cos 2\beta_1 \operatorname{sign}(\dot{\gamma}^{(2)})] \tag{45a}$$

$$\tau_{tt} = E_1 \int_0^t (D_{tt} + D_{zz})\,\mathrm{d}t + \frac{\tau_0}{\sin 4\alpha}[\cos 2\beta_2 \operatorname{sign}(\dot{\gamma}^{(1)}) - \cos 2\beta_1 \operatorname{sign}(\dot{\gamma}^{(2)})] \tag{45b}$$

$$\tau_{tz} = \frac{\tau_0}{\sin 4\alpha}[\sin 2\beta_1 \operatorname{sign}(\dot{\gamma}^{(2)}) - \sin 2\beta_2 \operatorname{sign}(\dot{\gamma}^{(1)})]. \tag{45c}$$

The integral on the right hand side of equations (45a) and (45b) is zero for simple shear due to $D_{tt} = D_{zz} = 0$. It is also zero in the case of pure torsion due to the relation $D_{tt} + D_{zz} = 0$. However, it is not zero for simple torsion because $D_{tt} \neq 0$. The macroscopic stress components corresponding to the aforementioned microscopic quantities are then obtained by orientation averaging, given by (20a), (20b) and (20c). By use of (45), these equations are integrated. The procedure of integration is similar to the one used by Dafalias (1993a), and the resulting stress components for the unified solution are obtained as

$$\sigma_{zz} = E_1 \int_0^t \xi D_{tt}\,\mathrm{d}t + \frac{\tau_0}{2\pi(b^2+c^2)}\left\{\sin^2 2\psi\left[\left(\frac{c}{\cos 2\alpha} - \frac{b}{\sin 2\alpha}\right)\ln L_1 + \left(\frac{c}{\cos 2\alpha} + \frac{b}{\sin 2\alpha}\right)\ln L_2\right]\right.$$
$$\left. + 2a\left[\left(\frac{c}{\sin 2\alpha} + \frac{b}{\cos 2\alpha}\right)\left(\tan^{-1} T_1 - \frac{\pi}{2}\right) - \left(\frac{c}{\sin 2\alpha} - \frac{b}{\cos 2\alpha}\right)\left(\tan^{-1} T_2 + \frac{\pi}{2}\right)\right]\right\} \tag{46a}$$

$$\sigma_{tt} = E_1 \int_0^t \xi D_{tt}\,\mathrm{d}t - \frac{\tau_0}{2\pi(b^2+c^2)}\left\{\sin^2 2\psi\left[\left(\frac{c}{\cos 2\alpha} - \frac{b}{\sin 2\alpha}\right)\ln L_1 + \left(\frac{c}{\cos 2\alpha} + \frac{b}{\sin 2\alpha}\right)\ln L_2\right]\right.$$
$$\left. + 2a\left[\left(\frac{c}{\sin 2\alpha} + \frac{b}{\cos 2\alpha}\right)\left(\tan^{-1} T_1 - \frac{\pi}{2}\right) - \left(\frac{c}{\sin 2\alpha} - \frac{b}{\cos 2\alpha}\right)\left(\tan^{-1} T_2 + \frac{\pi}{2}\right)\right]\right\} \tag{46b}$$

$$\sigma_{tz} = \frac{\tau_0}{2\pi(b^2+c^2)}\left\{\sin^2 2\psi\left[\left(\frac{c}{\sin 2\alpha} + \frac{b}{\cos 2\alpha}\right)\ln L_1 - \left(\frac{c}{\sin 2\alpha} - \frac{b}{\cos 2\alpha}\right)\ln L_2\right]\right.$$
$$\left. - 2a\left[\left(\frac{c}{\cos 2\alpha} - \frac{b}{\sin 2\alpha}\right)\left(\tan^{-1} T_1 - \frac{\pi}{2}\right) + \left(\frac{c}{\cos 2\alpha} + \frac{b}{\sin 2\alpha}\right)\left(\tan^{-1} T_2 + \frac{\pi}{2}\right)\right]\right\} \tag{46c}$$

where

$$L_1 = \frac{a + b\sin(2\alpha - 2\phi) + c\cos(2\alpha - 2\phi)}{a - b\sin(2\alpha - 2\phi) - c\cos(2\alpha - 2\phi)}; \quad L_2 = \frac{a + b\sin(2\alpha + 2\phi) - c\cos(2\alpha - 2\phi)}{a - b\sin(2\alpha + 2\phi) + c\cos(2\alpha + 2\phi)} \tag{46d}$$

$$T_1 = \frac{\sin^2 2\psi}{c\sin(2\alpha - 2\phi) - b\cos(2\alpha - 2\phi)}; \quad T_2 = \frac{\sin^2 2\psi}{c\sin(2\alpha + 2\phi) + b\cos(2\alpha + 2\phi)} \tag{46e}$$

$$\begin{cases} a = [\sin^2 2\psi + 2\sinh^2(\frac{1}{2}\Gamma t)] \\ b = 2\sinh(\frac{1}{2}\Gamma t)[\sinh(\frac{1}{2}\Gamma t)\cos 2\psi \sin 2\phi - \cosh(\frac{1}{2}\Gamma t)\sin 2\psi \cos 2\phi] \\ c = -2\sinh(\frac{1}{2}\Gamma t)[\sinh(\frac{1}{2}\Gamma t)\cos 2\psi \cos 2\phi + \cosh(\frac{1}{2}\Gamma t)\sin 2\psi \sin 2\phi] \end{cases} \tag{46f}$$

and

$$\Gamma = 2D_{tz}\tan(2\psi), \quad \cos 2\psi = \cos 2\alpha \cos 2\phi, \quad \tan 2\phi = -\zeta\frac{D_{tt}}{D_{tz}}. \tag{46g}$$

The parameter ξ that appears in (46a, b) is equal to one for simple torsion and equal to zero for both simple shear and pure torsion. The other parameter ζ has already been defined

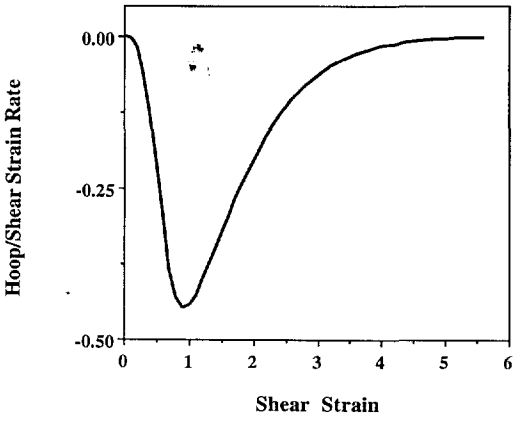

Fig. 2. Hoop strain rate vs shear strain during pure torsion of elastic perfectly plastic material.

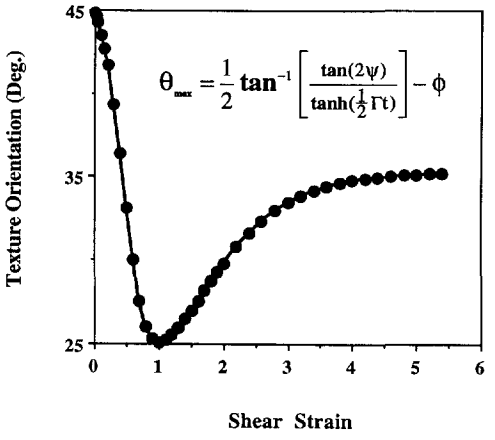

Fig. 3. Ideal orientation of texture during pure torsion of elastic perfectly plastic material.

in (43b), and also depends on the geometry and loading condition of the problem. It is noted that the expressions of T_1 and T_2 in (46e) are different from those of Dafalias (1993a) in order to avoid the jump in value of the inverse tangent function during deformation.

The hoop strain rate D_{tt} is zero in the case of simple shear but it is not zero in both cases of torsion. In the latter cases, it is determined by the geometrically symmetrical condition of $\sigma_{tt} = 0$ from (46b). D_{tt} may be determined for each shear strain $2D_{tz}t$ by use of a numerical procedure to find zeroes, using the non-linear equation obtained by setting $\sigma_{tt} = 0$ in (46b).

Figure 2 shows the numerical results of torsion of a thin-walled tube with free-end, in which the ratio D_{tt}/D_{tz} increases from zero to a maximum value as the shear strain increases, and it decreases thereafter and gets back to zero. An interesting result from this calculation is that the variation of hoop strain rate is closely tied to a fascinating phenomenon in the rotation of ideal orientation shown in Fig. 3. It is seen that the variation of ideal orientation specified by angle θ_{max} as the shear strain increases is parallel with the variation of the D_{tt}/D_{tz} ratio. The expression for θ_{max} given in Fig. 3 is found from $\partial f/\partial\theta = 0$, where f is obtained by replacing θ in (38a) by $\theta+\phi$. Figure 4 describes more clearly the shifting of the peak of the ODF as the shear strain increases in magnitude from zero. The curves show the ODF variation for each constant shear strain level, given by numbers in the figure. At the beginning, the value of the ODF is one for all angles. As the shear strain increases, a peak of the ODF curve gradually forms and it gradually shifts to the left at the low and medium shear strain level. The direction of shifting takes a turn at the shear strain of approximately equal to 1.0 and then the peak shifts to the right at the larger shear strain level. This shifting of the ideal orientation is also referred to as the "tilting" phenomenon (Montheillet, *et al.*, 1984, 1985; Toth *et al.*, 1992). Some remarks concerning the tilting

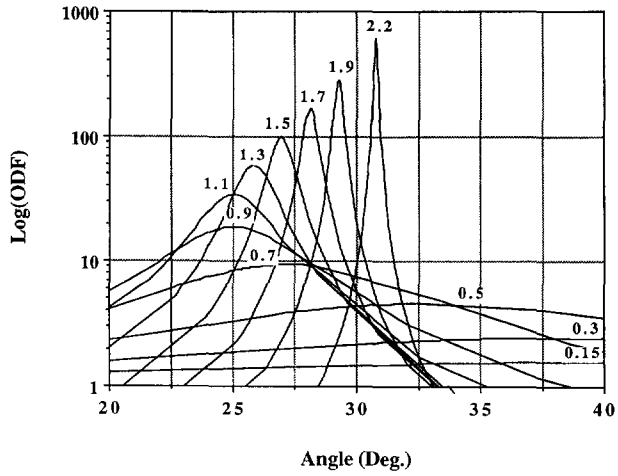

Fig. 4. ODF distribution at different shear strain levels in pure torsion of elastic perfectly plastic material.

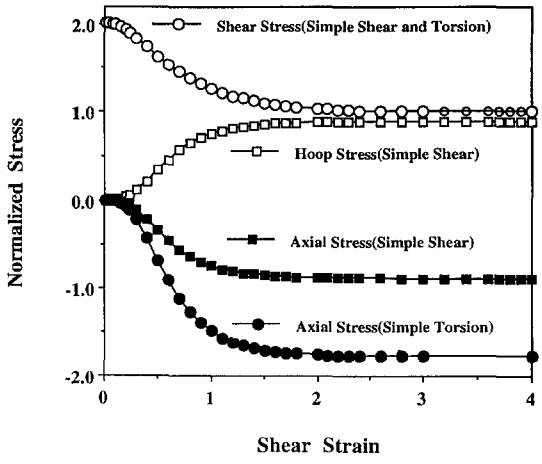

Fig. 5. Normalized stresses for three different problems for elastic perfectly plastic material.

and a comparison of the theoretical prediction with the experimental results will be given in Section 7.

Another basic finding of this study is that the axial stress for simple torsion is exactly two times as large as that for simple shear, as shown in Fig. 5 (the stress is normalized with respect to τ_0). This effect is independent of strain hardening and will be further discussed in the next section. This finding agrees with the result obtained from the computer simulation of texture evolution carried out by Harren *et al.* (1989). Figure 6 shows the ratio R obtained from Harren *et al.* (1989) plotted against the shear strain. Due to the relation $\sigma^s_{11} = -\sigma^s_{22}$ for simple shear, the ratio $R = (\sigma^s_{22} - \sigma^s_{11})/|\sigma^t_{11}|$ is equal to one if the axial stress for simple torsion is exactly two times as large as that for simple shear as aforementioned. In the above definition of R, the superscript "s" denotes the simple shear and the superscript "t" denotes torsion. It is seen from Fig. 6 that the ratio R is close to the one for the 489-grain simulation. It is close to the one for the 300-grain simulation up to a strain of 2.0 and then increases somewhat. A conclusion can therefore be drawn from this finding that, in the verification test, the theoretical axial stress for simple shear should be compared with half of the experimental value (rather than the whole value as it is usually done in the literature) obtained from fixed-end torsion test of a thin-walled tube. Further discussion about this point will be given in Section 7. Figure 5 also shows that while the hoop stress is zero for simple torsion, it is not zero for simple shear; and the shear stress–strain curves for all three cases are practically identical. Note that all stresses are normalized with respect to τ_0.

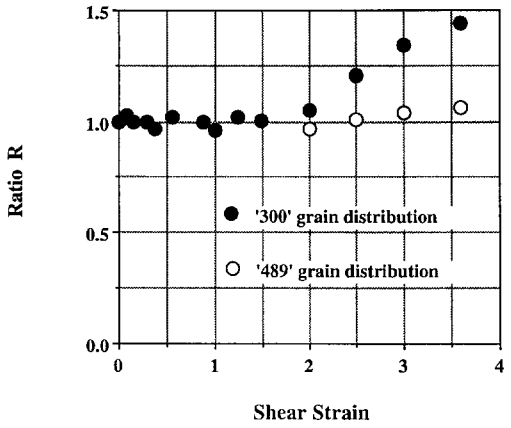

Fig. 6. Axial stress ratio determined from Harren *et al.* (1989).

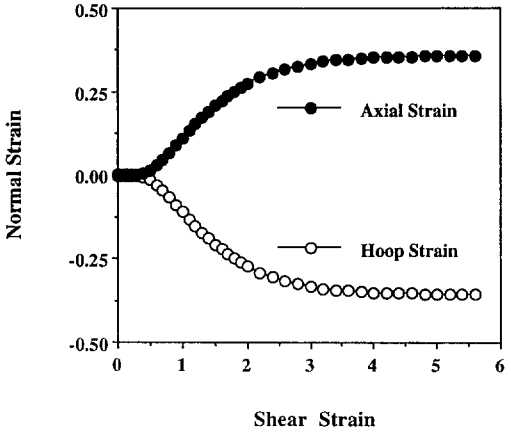

Fig. 7. Hoop and axial strains in pure torsion of elastic perfectly plastic material.

Finally, Fig. 7 shows the axial and hoop strains in pure torsion. Three stages may be observed from this figure. The first stage incurs small axial and hoop strains, resulting in only slight change in texture. This may be observed from Fig. 4 where the ODF value is slightly larger than one. The second stage is a texture formation stage, where the axial and hoop strain increase rapidly during torsion. The corresponding shear strain is approximately from 0.5 to 2.0. It is within this stage that the ideal orientation angle shifts back and forth, see Fig. 3, and the ODF has a rapid increase in value, see Fig. 4. In the third stage, the texture stabilizes and the growth of axial and hoop strains slows down to a zero rate.

6. UNIFIED SOLUTION FOR HARDENING MATERIALS

In this section, a unified solution is derived for materials with strain-hardening defined by (16) and (3), but using condition (28) for simplification. In this case, the strain-hardening is represented by

$$\tau^{(1)} = h(\dot{\gamma}^{(1)} + q_1\dot{\gamma}^{(2)}), \quad \dot{\tau}^{(2)} = h(q_1\dot{\gamma}^{(1)} + \dot{\gamma}^{(2)}) \tag{47a,b}$$

with a sign term for positive and/or negative slip, such that

$$q_I = q\,\mathrm{sign}(\dot\gamma^{(1)}\dot\gamma^{(2)}). \tag{47c}$$

Using a similar procedure as that which led to (32) and the conditions (39)–(41) of simple shear, simple torsion and pure torsion, the following expressions are obtained

$$\dot\gamma^{(1)} = \frac{1}{\sin 4\alpha}[(1-Q_I)\zeta D_{tt}\cos 2\alpha\cos 2\theta + (1-H_I)\zeta D_{tt}\sin 2\alpha\sin 2\theta$$
$$-2(1-Q_I)D_{tz}\cos 2\alpha\sin 2\theta + 2(1-H_I)D_{tz}\sin 2\alpha\cos 2\theta] \tag{48a}$$

$$\dot\gamma^{(2)} = \frac{1}{\sin 4\alpha}[-(1-Q_I)\zeta D_{tt}\cos 2\alpha\cos 2\theta + (1-H_I)\zeta D_{tt}\sin 2\alpha\sin 2\theta$$
$$+2(1-Q_I)D_{tz}\cos 2\alpha\sin 2\theta + 2(1-H_I)D_{tz}\sin 2\alpha\cos 2\theta] \tag{48b}$$

where

$$H_I = \frac{\frac{h}{2\mu}(1+q_I)\left[1-\cos 4\alpha + \frac{h}{\mu}(1-q_I)\right]}{\eta + \frac{h}{\mu}(1-q_I\cos 4\alpha) + \frac{1}{2}\left(\frac{h}{\mu}\right)^2(1-q_I^2)} \tag{48c}$$

$$Q_I = \frac{\frac{h}{2\mu}(1-q_I)\left[1+\cos 4\alpha + \frac{h}{\mu}(1+q_I)\right]}{\eta + \frac{h}{\mu}(1-q_I\cos 4\alpha) + \frac{1}{2}\left(\frac{h}{\mu}\right)^2(1-q_I^2)}. \tag{48d}$$

These equations may then be used to obtain

$$\dot\theta_I = \frac{D_{tz}}{\cos 2\psi_I}[\cos(2\theta+2\phi) - \cos 2\psi_I], \quad \cos 2\psi_I = \frac{\cos 2\alpha\cos 2\phi}{1-H_I}, \quad \tan 2\phi = -\zeta\frac{D_{tt}}{D_{tz}}. \tag{49}$$

Note that eqns (32) and (33) presented in Section 4 for simple shear are recovered by setting $q_I = q$, $\zeta = 0$, and $\phi = 0$ in eqns (48) and (49).

From (49), the ideal orientation θ_s is

$$\theta_s = \psi_I - \phi. \tag{50}$$

It is obvious from (49) and (50) that two factors are affecting the ideal orientation. They are the crystal hardening parameter H_I and the hoop strain rate D_{tt}.

From (47) and (16) the resolved shear stresses are

$$\tau^{(1)} = \tau_0\,\mathrm{sign}(\dot\gamma^{(1)}) + \int_0^t h(t)[\dot\gamma^{(1)} + q_I\dot\gamma^{(2)}]\,\mathrm{d}t \tag{51a}$$

$$\tau^{(2)} = \tau_0\,\mathrm{sign}(\dot\gamma^{(2)}) + \int_0^t h(t)[q_I\dot\gamma^{(1)} + \dot\gamma^{(2)}]\,\mathrm{d}t. \tag{51b}$$

After the substitution of (51) and (48) into (13), the local stress components are found to be

$$\tau_{zz} = E_1 \int_0^t (D_{rr} + D_{zz})\,\mathrm{d}t - \frac{\tau_0}{\sin 4\alpha}[\cos 2\beta_2\ \mathrm{sign}(\dot{\gamma}^{(1)}) - \cos 2\beta_1\ \mathrm{sign}(\dot{\gamma}^{(2)})]$$
$$- \frac{1}{\eta}\int_0^t h\zeta D_{rr}[(1-H_I)(1+q_I)(\sin 2\alpha)^2 + (1-Q_I)(1-q_I)(\cos 2\alpha)^2]\,\mathrm{d}t$$
$$- \frac{1}{\eta}\int_0^t h[(1-H_I)(1+q_I)(\sin 2\alpha)^2 - (1-Q_I)(1-q_I)(\cos 2\alpha)^2](D_{rz}\sin 4\theta - \zeta D_{rr}\cos 4\theta)\,\mathrm{d}t \tag{52a}$$

$$\tau_{rr} = E_1 \int_0^t (D_{rr} + D_{zz})\,\mathrm{d}t + \frac{\tau_0}{\sin 4\alpha}[\cos 2\beta_2\ \mathrm{sign}(\dot{\gamma}^{(1)}) - \cos 2\beta_1\ \mathrm{sign}(\dot{\gamma}^{(2)})]$$
$$+ \frac{1}{\eta}\int_0^t h\zeta D_{rr}[(1-H_I)(1+q_I)(\sin 2\alpha)^2 + (1-Q_I)(1-q_I)(\cos 2\alpha)^2]\,\mathrm{d}t$$
$$+ \frac{1}{\eta}\int_0^t h[(1-H_I)(1+q_I)(\sin 2\alpha)^2 - (1-Q_I)(1-q_I)(\cos 2\alpha)^2](D_{rz}\sin 4\theta - \zeta D_{rr}\cos 4\theta)\,\mathrm{d}t \tag{52b}$$

$$\tau_{rz} = \frac{\tau_0}{\sin 4\alpha}[\sin 2\beta_1\ \mathrm{sign}(\dot{\gamma}^{(2)}) - \sin 2\beta_2\ \mathrm{sign}(\dot{\gamma}^{(1)})]$$
$$+ \frac{1}{\eta}\int_0^t hD_{rz}[(1-H_I)(1+q_I)(\sin 2\alpha)^2 + (1-Q_I)(1-q_I)(\cos 2\alpha)^2]\,\mathrm{d}t$$
$$+ \frac{1}{\eta}\int_0^t h[(1-H_1)(1+q_I)(\sin 2\alpha)^2 - (1-Q_I)(1-q_I)(\cos 2\alpha)^2](D_{rz}\cos 4\theta + \zeta D_{rr}\sin 4\theta)\,\mathrm{d}t. \tag{52c}$$

The macroscopic stress components are obtained by the ODF averaging on all orientations. The integration of the first and second terms of (52) has already been carried out in (46). The integration of the third term is simple due to its independence of ODF. The integration of the fourth term of each stress component of (52) is quite lengthy and the details will not be given here. The expressions presented here represent macroscopic stresses obtained by considering only the self-hardening. The effect of latent hardening is neglected, i.e., $q = 0$. In this case, (20) gives

$$\boldsymbol{\sigma}_{zz} = E_1 \int_0^t \xi D_{rr}\,\mathrm{d}t - \frac{\tau_0}{2\pi(b^2+c^2)}\left\{\sin^2\psi\left[\left(\frac{c}{\cos 2\alpha} - \frac{b}{\sin 2\alpha}\right)\ln L_{S1} + \left(\frac{c}{\cos 2\alpha} + \frac{b}{\sin 2\alpha}\right)\ln L_{S2}\right]\right.$$
$$\left. + 2a\left[\left(\frac{c}{\sin 2\alpha} + \frac{b}{\cos 2\alpha}\right)\left(\tan^{-1} T_{S1} - \frac{\pi}{2}\right) - \left(\frac{c}{\sin 2\alpha} - \frac{b}{\cos 2\alpha}\right)\left(\tan^{-1} T_{S2} + \frac{\pi}{2}\right)\right]\right\}$$
$$- \frac{1}{\eta}\int_0^t h[(1-H_S)\sin^2 2\alpha + (1-Q_S)\cos^2 2\alpha]\zeta D_{rr}\,\mathrm{d}t$$
$$- \frac{1}{\eta}\int_0^t h[(1-H_S)\sin^2 2\alpha - (1-Q_S)\cos^2 2\alpha](D_{rz}T_{S3} - \zeta D_{rr}T_{S4})\,\mathrm{d}t \tag{53a}$$

$$\boldsymbol{\sigma}_{rr} = E_1 \int_0^t \xi D_{rr}\,\mathrm{d}t - \frac{\tau_0}{2\pi(b^2+c^2)}\left\{\sin^2 2\psi\left[\left(\frac{c}{\cos 2\alpha} - \frac{b}{\sin 2\alpha}\right)\ln L_{S1}\right.\right.$$

$$+\left(\frac{c}{\cos 2\alpha}+\frac{b}{\sin 2\alpha}\right)\ln L_{S2}\Bigg]+2a\Bigg[\left(\frac{c}{\sin 2\alpha}+\frac{b}{\cos 2\alpha}\right)\left(\tan^{-1}T_{S1}-\frac{\pi}{2}\right)$$

$$-\left(\frac{c}{\sin 2\alpha}-\frac{b}{\cos 2\alpha}\right)\left(\tan^{-1}T_{S2}+\frac{\pi}{2}\right)\Bigg]\Bigg\}$$

$$+\frac{1}{\eta}\int_0^t h[(1-H_S)\sin^2 2\alpha+(1-Q_S)\cos^2 2\alpha]\zeta D_{tt}\,\mathrm{d}t$$

$$+\frac{1}{\eta}\int_0^t h[(1-H_S)\sin^2 2\alpha-(1-Q_S)\cos^2 2\alpha](D_{tz}T_{S3}-\zeta D_{tt}T_{S4})\,\mathrm{d}t \tag{53b}$$

$$\sigma_{tz}=\frac{\tau_0}{2\pi(b^2+c^2)}\Bigg\{\sin^2 2\psi\Bigg[\left(\frac{c}{\sin 2\alpha}+\frac{b}{\cos 2\alpha}\right)\ln L_{S1}-\left(\frac{c}{\sin 2\alpha}-\frac{b}{\cos 2\alpha}\right)\ln L_{S2}\Bigg]$$

$$-2a\Bigg[\left(\frac{c}{\cos 2\alpha}-\frac{b}{\sin 2\alpha}\right)\left(\tan^{-1}T_{S1}-\frac{\pi}{2}\right)+\left(\frac{c}{\cos 2\alpha}+\frac{b}{\sin 2\alpha}\right)\left(\tan^{-1}T_{S2}+\frac{\pi}{2}\right)\Bigg]\Bigg\}$$

$$+\frac{1}{\eta}\int_0^t h[(1-H_S)\sin^2 2\alpha+(1-Q_S)\cos^2 2\alpha]D_{tz}\,\mathrm{d}t$$

$$+\frac{1}{\eta}\int_0^t h[(1-H_S)\sin^2 2\alpha-(1-Q_S)\cos^2 2\alpha](D_{tz}T_{S4}+\zeta D_{tt}T_{S3})\,\mathrm{d}t \tag{53c}$$

with

$$L_{S1}=\frac{a+b\sin(2\beta-2\phi)+c\cos(2\beta-2\phi)}{a-b\sin(2\beta-2\phi)-c\cos(2\beta-2\phi)};\quad L_{S2}=\frac{a+b\sin(2\beta+2\phi)-c\cos(2\beta+2\phi)}{a-b\sin(2\beta+2\phi)+c\cos(2\beta+2\phi)} \tag{53d}$$

$$T_{S1}=\frac{\sin^2 2\psi}{c\sin(2\beta-2\phi)-b\cos(2\beta-2\phi)};\quad T_{S2}=\frac{\sin^2 2\psi}{c\sin(2\beta+2\phi)+b\cos(2\beta+2\phi)} \tag{53e}$$

$$T_{S3}=\frac{2bc(a^2-2a\sin^2 2\psi-\sin^4 2\psi)}{(b^2+c^2)^2};\quad T_{S4}=\frac{(c^2-b^2)(a^2-2a\sin^2 2\psi-\sin^4 2\psi)}{(b^2+c^2)^2} \tag{53f}$$

$$H_S=\frac{\frac{h}{2\mu}\left[1-\cos 4\alpha+\frac{h}{\mu}\right]}{\eta+\frac{h}{\mu}+\frac{1}{2}\left(\frac{h}{\mu}\right)^2},\quad Q_S=\frac{\frac{h}{2\mu}\left[1+\cos 4\alpha+\frac{h}{\mu}\right]}{\eta+\frac{h}{\mu}+\frac{1}{2}\left(\frac{h}{\mu}\right)^2},\quad \tan 2\beta=\frac{1-H_S}{1-Q_S}\tan 2\alpha. \tag{53g}$$

There are, in general, four terms in each of the stress components in (52) and (53). They represent, respectively, the elastic response, the texture softening, the pure strain hardening, and the interaction between texture softening and strain hardening. Thus, in a special case, the equations the elastic perfectly-plastic material are recovered by setting h to zero, i.e., (52) reduces to (45) and (53) reduces to (46), where the effect of pure strain hardening and its coupling with texture softening disappear.

The above expressions are now applied to investigate simple and pure torsion tests of a high purity aluminum, which is a nonlinearly hardening material. Experimental data are reported in Wu *et al.* (1993, 1995b). The experimental shear stress–strain curves of this

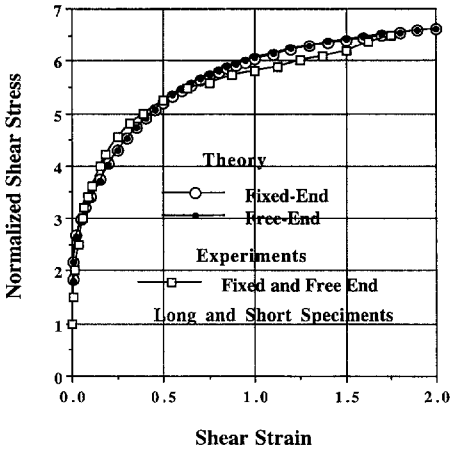

Fig. 8. Normalized shear stress–strain curves for high purity aluminum.

material at room temperature are shown in Fig. 8, in which the theoretical results are also shown. Note that the stresses are normalized with respect to τ_0 (10 MPa) in this discussion and the shear stress–strain curves for the two cases of torsion are indistinguishable. In the theoretical work, the following simple expression of hardening modulus is used

$$h(t) = h_S + \sum_{k=1}^{4} h_k \exp(-a_k \varepsilon), \quad \varepsilon = 2\int D_{12}\, dt. \tag{54a}$$

The associated material constants used in the calculation are chosen as

$$\begin{aligned} h_S &= 1.0(\text{MPa}) \\ h_k &= (1\times 10^4, 8\times 10^2, 40.0, 8.0)(\text{MPa}) \\ a_k &= (1\times 10^3, 50.0, 1.5, 0.55) \end{aligned} \tag{54b}$$

where $k = 1, 2, 3$, and 4. Note that a different functional form may be used in (54) with different constants, as long as it describes the same hardening behavior (same curve) as that described by (54a, b). The specific mathematical expression of (54) should not have any effect on the texture evolution and texture induced axial effect. The elastic constants are $\mu = 6.83\times 10^4$ MPa and ν (Poisson's ratio) $= 0.345$.

The theoretical normalized axial stress incurred in simple torsion is compared with the corresponding experimental data in Fig. 9. The theoretical result depends on the characteristic angle α of the double-slip system. The result obtained by use of $\alpha = 23.70$ degrees

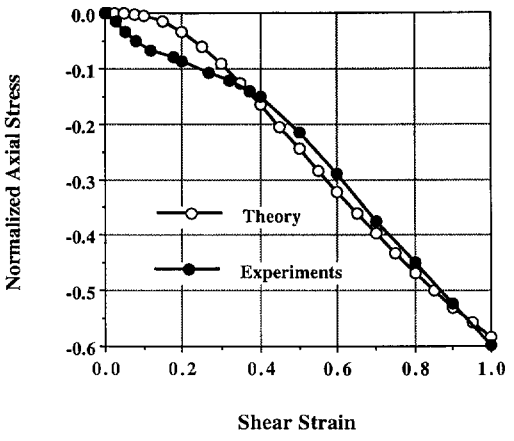

Fig. 9. Axial stress in simple torsion for aluminum.

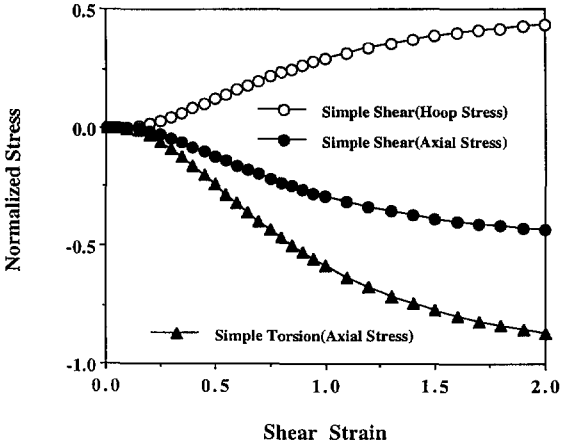

Fig. 10. Stress components for simple shear and simple torsion for aluminum.

matches experimental data the best and is presented in this figure. It is seen that there is a general agreement between theory and experiment except for the early stage of deformation, when shear strain is less than 0.35. A possible reason for the discrepancy is that the double-slip model does not realistically describe the slip systems at this moderate strain range. In this range, multislip usually occurs. Nevertheless, the results do show that the double-slip model can lead to a reasonable result at the large stain level.

Figure 10 shows that the axial stress of simple torsion is two times as large as that of simple shear. The hoop stress σ_{22} is zero for simple torsion and is not zero for simple shear. In fact, these relations may be derived easily from (53a, b), independent of whether the material is of strain-hardening type or non-hardening type. From these equations, the stress components are

$$\boldsymbol{\sigma}_{zz} = E_1 \int \xi D_{tt}\, \mathrm{d}t + \Sigma \tag{55a}$$

$$\boldsymbol{\sigma}_{tt} = E_1 \int \xi D_{tt}\, \mathrm{d}t - \Sigma \tag{55b}$$

where Σ represents the remaining terms in the expressions for (53a, b). In the case of simple shear, $D_{tt} = 0$ and (55) leads to

$$\boldsymbol{\sigma}_{zz} = -\boldsymbol{\sigma}_{tt} = \Sigma. \tag{56}$$

On the other hand $D_{tt} \neq 0$ in simple torsion. With $\xi = 1$ and $\boldsymbol{\sigma}_{tt} = 0$, (55b) is then reduced to

$$\Sigma = E_1 \int \xi D_{tt}\, \mathrm{d}t. \tag{57}$$

Thus, from (55a), the axial stress is given by

$$\boldsymbol{\sigma}_{zz} = 2\Sigma \tag{58}$$

which is twice as large as the axial stress in (56). The same conclusion was also obtained by Harren *et al.* (1989) based on a phenomenological hyperelastic constitutive model.

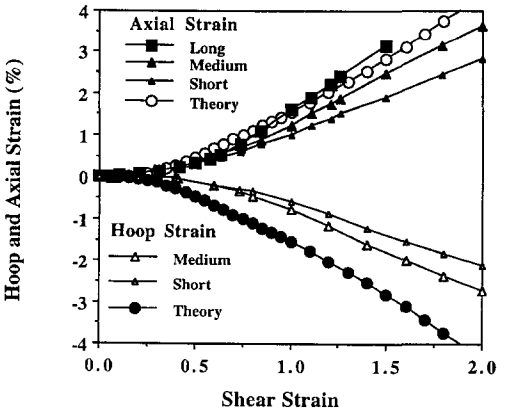

Fig. 11. Hoop and axial strains in pure torsion of aluminum.

Figure 11 shows a good agreement, in axial and hoop strains, between experimental results and theoretical predictions for pure torsion. Some differences in the hoop strain are found which result from the approximation of $D^p_{rr} = 0$ in the theory. Another source of discrepancy comes from the experimental side. It has been shown in Wu *et al.* (1993, 1995b) that the gauge length of the tubular specimen greatly affects the axial and hoop strains for the range of gauge lengths tested. The longer the gauge length is the closer are the experimental results to the true values. In this figure, the theoretical result of the axial strain has been compared to data of long specimens. However, the hoop strain has not been experimentally determined by use of long specimens. The data presented are for medium and short specimens. Had there been data for long specimens, the agreement in the hoop strain would have been much improved. An interesting observation is that the axial and hoop strain increments approximate a constant in the shear strain range between 0.75 and 1.75. It may be seen from (53b) that this effect indicates a balance between the texture softening and strain hardening in this shear strain range. Comparing Fig. 11 with Fig. 7 (note that the strain scales are different in the two figures), it may be concluded that strain-hardening delays the development of axial and hoop strains. Figure 12 shows the ideal orientation of this (strain-hardening) material plotted against shear strain in the case of free-end torsion. It is seen, by comparing this figure with Fig. 3, that the peak of the curve has moved from about 1.0 in Fig. 3 to the current 2.0. This implies that the formation of textures is delayed by strain-hardening. Furthermore, Fig. 12 shows that the "tilting" is about ± 0.5 degrees which is much smaller than the tilting of ± 10 degrees in Fig. 3. In addition, it should be stated, as it has already been mentioned in Section 5, that texture formation can increase the development of axial and hoop strains. Therefore, the early development of the axial and hoop strains in an extruded specimen as observed by Wu *et al.* (1993, 1995b) can be explained.

7. DISCUSSION AND CONCLUSION

7.1. *Crystal elasticity*

The consideration of crystal elasticity is important in that the general planar stress and strain states may be determined. Moreover, as discussed by Lowe and Lipkin (1990), elasticity may play a key role in the axial stress response during reverse torsion. This point is significant in the light of a common tendency by researchers to assume that elasticity is of minor importance and hence can be neglected in the analysis of large-strain deformation. In this paper, eqns (46) and (53) show that the first term (the "elastic texture" term), which represents the elastic stress caused by the inelastic hoop strain developed due to texture formation, appears in the expressions for axial and hoop stresses but not in the expression for shear stress. This elastic texture term is thus instrumental in the development of axial stress and hoop strain. In the case of simple torsion, (55a) and (57) show that the elastic texture term is equal in magnitude to the texture evolution term, i.e., the crystal elasticity

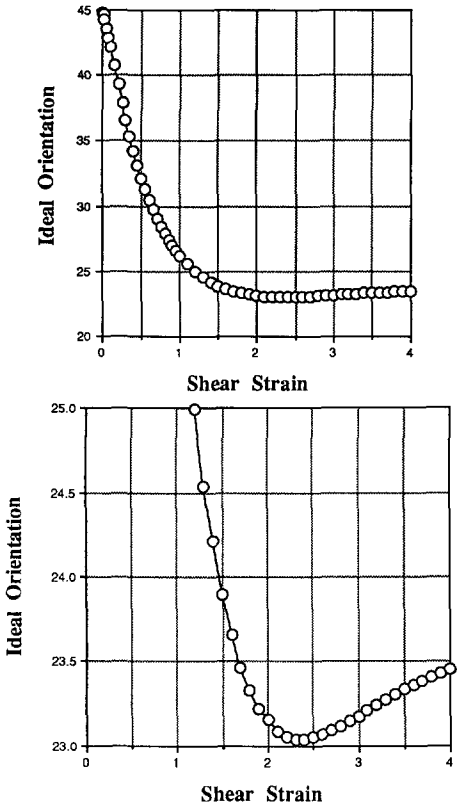

Fig. 12. Ideal orientation of texture during pure torsion of aluminum.

and the texture evolution are of equal importance as far as the axial stress development is concerned. Equations (55)–(58) indicate clearly that the axial stress in simple torsion is twice that in simple shear due to the coupling of crystal elasticity with boundary condition, i.e., the effect of the elastic texture term. This result confirms the assertion of Lowe & Lipkin (1990) that axial stress is as sensitive to boundary condition as it is to texture induced anisotropy. A further remark concerns the present treatment of isotropic crystal elasticity instead of the realistic anisotropic crystal elasticity. This is a reasonable approximation and it greatly reduces the complexity of texture analysis. According to the computer analysis of Lowe and Lipkin (1990), using a polycrystal model code developed by Asaro and Needleman (1985) and inputting isotropic and/or anisotropic elastic constants, the overall response of axial stress is similar for the two cases. This is so even in the case of reverse torsion and use of different axial stiffness. A further approximation has been made in this work concerning the lattice spin due to crystal elastic stretch. Such spin is neglected compared with the large lattice spin due to rigid body rotation under the assumption of small lattice strain.

7.2. *Rotation of ideal orientation during torsion*

The phenomenon of "tilting" or rotation of pole figures about the radial (r) axis during torsion was reported experimentally by Motheillet *et al.* (1984) for fixed end torsion, and by Toth *et al.* (1992) for free end torsion, both for solid bars. It was observed that the tilting of the ideal orientation was opposite in direction to shear at low strain and then changed into the direction of shear at large strain. Stout and O'Rourke (1989) tested thin-walled tubes of the Lindholm configuration in free-end torsion with a lubricated mandrel and reported an experimental (111) pole figure of OFE copper, which rotated about the r-axis, opposite to the shear direction, at a shear strain of 1.5. Wang *et al.* (1995) tested long gauge-length, thick-walled tubes in free-end torsion and the pole figures also showed the tilting effect. The experimental angle of tilting is small, depending on the material and test condition. It was in the range of $\pm 5^\circ$ in Montheillet *et al.* (1985), and $-3^\circ \sim +2^\circ$ in Toth

et al. (1992) for A, B, C components of ideal orientation at room temperature, 125°C, 200°C and 300°C. It was about 5° in Wang *et al.* (1995).

The tilting was found in a computer simulation of torsion, based on Taylor and relaxed constraint theory, carried out by Canova *et al.* (1984, 1985). This effect was explained and related closely to the development of axial effect by means of the simplified rate-independent theory (Montheillet *et al.*, 1985) and the rate dependent theory (Toth *et al.*, 1988, 1989, 1990). The "tilting" in the amount of $-7°$ at a shear strain of 3.6 was also found by Harren *et al.* (1989) in a computer simulation of free-end torsion of a tubular specimen.

The analytical solution of the present paper correctly predicts the tilting effect. This agreement with experimental observation is demonstrated through Figs 3 and 4. The figures show that the peak of ODF shifts from 45° to 25° as the shear strain increases from zero to about 1.0. During this stage, the rotation is in the direction from the t-axis to the z-axis, which is opposite to the direction of shear. When the shear strain is greater than 1.0 the peak of ODF moves from 25° to 35°, in the direction of shear. This directional change of rotation is completely consistent with the aforementioned experimental finding. Furthermore, the present theory predicts that the magnitude of tilting depends greatly on crystal hardening, and that the maximum is $\pm 10°$ for elastic-perfectly plasticity material in free-end torsion. But, when material hardening is considered, the magnitude of tilting will decrease, to about $\pm 1°$ for aluminum, and the shear strain level at which the tilting changes direction will increase to about 2.0, as shown in Fig. 12 for high purity aluminum (a material with crystal hardening). A relation between tilting and axial effect is obtained through a connection with hoop strain, which is shown in Figs 2 and 13 to be directly related to the texture formation and evolution. Note that, in the case of pure torsion, the axial strain is directly connected to hoop strain through the relation of $D_{zz} = -D_{tt}$. In the case of simple torsion, the axial stress is induced by hoop strain through the elastic texture terms of (46) and (53). The shift of ideal orientation, or the tilting, can be seen obviously from eqns (43a), (49) and (50). It is fair to say that the present theory predicts a larger amount of tilting for free-end torsion than for fixed-end torsion, because the hoop strain rate develops faster in free-end torsion than in fixed-end torsion. The larger amount of tilting for free-end torsion than for fixed-end torsion is also reported by Canova *et al.* (1985).

7.3. *Modeling of simple shear by simple torsion*

Simple shear has been considered as a benchmark test problem to check the constitutive models undergoing finite deformation. Many researchers have then compared the results of simple shear with that obtained from simple torsion of a thin-walled tube. This remark addresses the question of how well can the simple torsion of thin-walled tubes simulate the condition of simple shear. In the opinion of White (1992), a *short* tubular specimen with massive shoulders will provide restraint against change in radius and is a good approximation for simple shear. However, in the opinion of the present authors, the aforementioned test condition is an approximation for simple torsion rather than for simple shear. In fact, it is not even a good approximation for simple torsion, because the axial stress in this case

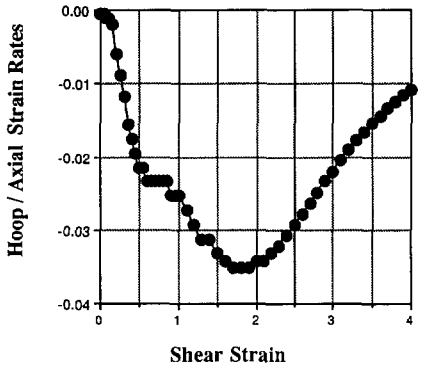

Fig. 13. Hoop strain rate vs shear strain during pure torsion of aluminum.

depends on gauge length and the axial stiffness of shoulder regions. The effect of shoulder regions on the axial stress can be discussed based on eqns (56) and (58).

As pointed out in Section 5, simple shear is quite different from simple torsion with different constraints and different stress and strain states. Moreover, it has been shown in Section 6 that the axial stress of simple torsion is twice as large as that of simple shear. The significance of this finding is that one should compare the theoretically predicted axial stress for simple shear with one-half of the experimental data obtained from simple torsion. In addition, the axial stress is as sensitive to boundary conditions as it is to texture induced anisotropy due to the elastic response term in the axial effect expression given by (46) and (53). This effect has already been discussed in Section 7.1 in connection with crystal elasticity.

7.4. *Plastic spin*

Plastic spin plays a key role in many recent macroscopic constitutive models and it provides insights that related microscopic to macroscopic aspects of large-strain plastic deformation, see, for instance, Dafalias (1985, 1993b), Van Der Giessen (1991), and others. Van Der Giessen (1989, 1991) defined an average plastic spin by ODF averaging as

$$\bar{W}^P_{12}(t) = \frac{1}{\pi}\int_{-\pi/2}^{\pi/2} W^P_{12} f(\theta, t)\,\mathrm{d}\theta, \quad W^P_{12} = \tfrac{1}{2}(\dot{\gamma}^{(1)} + \dot{\gamma}^{(2)}). \tag{59}$$

Using (48) and (49) and its related ODF expression, the integral in (59) may be integrated, and the following result is obtained

$$\frac{\bar{W}^P_{12}}{W_{12}} = \frac{\sinh^2(\frac{1}{2}\Gamma t)}{\sin^2 2\psi + \sinh^2(\frac{1}{2}\Gamma t)}, \quad \cos 2\psi = \frac{\cos 2\alpha \cos 2\phi}{1 - H_S},$$

$$\tan 2\phi = -\zeta \frac{D_{11}}{D_{12}}, \quad \Gamma = 2D_{12}\tan 2\psi. \tag{60}$$

Figure 14 shows the evolution of average (macroscopic) plastic spin with respect to shear strain for the cases of simple shear, simple torsion, and pure torsion. The three cases do not show significant differences, only that pure torsion shows a slightly faster plastic spin evolution than the other cases. However, a substantial variation in the plastic spin accumulation is observed when a different characteristic angle α is assumed. The angle α is a material parameter, see Dafalias (1993a, 1993b), and may change with material and strain hardening in the spirit of double-slip equivalence of the actual crystal slip systems. The values of $\alpha = 24^\circ$ provides the best fit to axial stress of simple torsion for the nonlinearly

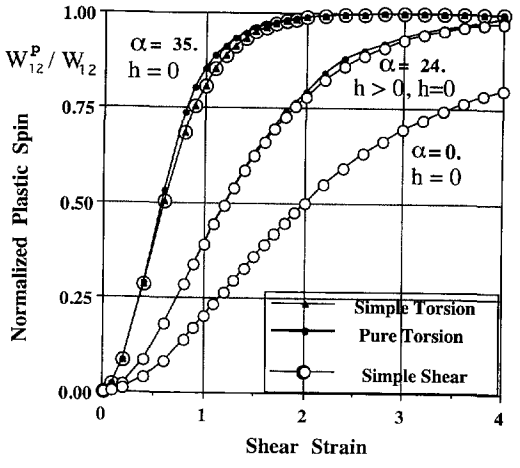

Fig. 14. The plastic spin.

hardening material (high purity aluminum) considered in this research. On the other hand, Dafalias (1993a) used $\alpha = 25°$ to describe experimental results of 1100-0 aluminum. Finally, it is noted that when $\alpha = 0$, the curve in Fig. 14 is identical with those obtained by Dafalias (1993b) and Van Der Giessen Van Houtte (1992) for single slip system.

7.5. *Conclusion*

It is shown in this paper that the double-slip model of crystal plasticity, when used together with the concept of ODF, describes the torsion tests very well, including the axial effects and texture orientation. This approach provides analytical solutions to the problems considered and provides valuable information for the macroscopic study of the constitutive equations.

Acknowledgements—The support by the CIFRE Fund of the University of Iowa and by the Alcoa Laboratories are greatly appreciated. One of the authors (Z.Q.) is partially supported by Special Grant KM85-33 of The Chinese Academy of Sciences.

REFERENCES

Asaro, R. J. (1983). Micro and macro mechanics of crystals and polycrystals. *Adv. Appl. Mech.* **23,** 1–100.

Asaro, R. J. and Needleman, A. (1985). Texture development and strain hardening in rate dependent polycrystals. *Acta Metall.* **33,** 923–953.

Asaro, R. J. and Rice, R. J. (1977). Strain localization in ductile single crystals. *J. Mech. Phys. Solids* **25,** 309–338.

Bronkhorst, C. A., Kalidindi, S. R. and Anand, L. (1992). Polycrystalline plasticity and the evolution of crystallographic texture in FCC metals. *Phil. Trans. R. Soc. Lond. A* **341,** 443–477.

Canova, G. R., Kocks, U. F. and Jonas, J. J. (1984). Theory of torsion texture development. *Acta Metall.* **32,** 211–226.

Canova, G. R., Kocks, U. F., Tome, C. N. and Jonas, J. J. (1985). The yield surface of textured polycrystals. *J. Mech. Phys. Solids* **33,** 371–397.

Clement, A. (1982). Prediction of deformation texture using a physical principle of conservation. *Mat. Sci. Engng* **55,** 203–210.

Dafalias, Y. F. (1985). The plastic spin. *ASME J. Appl. Mech.* **52,** 865–871.

Dafalias, Y. F. (1993a). Planar double-slip micromechanical model for polycrystal plasticity. *J. Engng Mechanics* **119,** 1260–1284.

Dafalias, Y. F. (1993b). On multiple spins and texture development. Case study: kinematic and orthotropic hardening. *Acta Mech.* **100,** 171–194.

Gilormini, P., Toth, L. S. and Jonas, J. J. (1990). An analytic method for the prediction of ODFS with application to the shear of FCC polycrystals. *Proc. R. Soc. Lond. A* **430,** 489–507.

Harren, S. V. and Asaro, R. J. (1989). Nonuniform deformations in polycrystals and aspects of the validity of the Taylor model. *J. Mech. Phys. Solids* **37,** 191–232.

Harren, S., Lowe, T. C., Asaro, R. J. and Needleman, A. (1989). Analysis of large-strain shear in rate-dependent face-centered cubic polycrystals: correlation of micro- and macromechanics. *Phil. Trans. R. Soc. Lond. A* **328,** 443–500.

Havner, K. S. and Salpekar, S. A. (1982). Theoretical latent hardening of crystals in double slip—I. F.C.C. crystals with a common slip plane. *J. Mech. Phys. Solids* **30,** 379–398.

Havner, K. S. and Salpekar, S. A. (1983). Theoretical latent hardening of crystals in double slip—II. F.C.C. crystals slipping on distinct planes. *J. Mech. Phys. Solids* **31,** 231–250.

Havner, K. S. (1992). *Finite Plastic Deformation of Crystalline Solids*, Cambridge University Press, New York.

Hill, R. (1966). Generalized constitutive relations for incremental deformation of metal crystals by multislip. *J. Mech. Phys. Solids* **14,** 95–102.

Hill, R. and Havner, K. S. (1982). Perspectives in the mechanics of elastoplastic crystals. *J. Mech. Phys. Solids* **30,** 5–22.

Hill, R. and Rice, J. R. (1972). Constitutive analysis of elastic-plastic crystals at arbitrary strain. *J. Mech. Phys. Solids* **20,** 401–413.

Lagzdins, A., Tamuzs, V., Teters, G. and Kregers, A. (1992). *Orientational Averaging in Mechanics of Solids*, Longman–John Wiley, New York.

Lin, T. H. (1964). Slip and stress fields of a polycrystalline aggregate at different stages of loading. *J. Mech. Phys. Solids* **12,** 391–408.

Lowe, T. C. and Lipkin, J. (1990). Analysis of axial deformation response during reverse shear. *SAND*90-8417, Technical report Sandia National Laboratories, Aberquerque. 1–36.

Montheillet, F., Cohen, M. and Jonas, J. J. (1984). Axial stresses and texture development during the torsion testing of Al, Cu and A-Fe. *Acta Metall.* **32,** 2077–2089.

Montheillet, F., Gilormini, P. and Jonas, J. J. (1985). Relation between axial stresses and texture development during torsion testing: a simplified theory. *Acta Metall.* **33,** 705–717.

Nemat-Nasser, S. and Obata, M. (1986). Rate-dependent, finite elasto-plastic deformation of polycrystals. *Proc. R. Soc. Lond. A* **407,** 343–375.

Prantil, V. C., Jenkins, J. T. and Dawson, P. R. (1993). An analysis of texture and plastic spin for planar polycrystals. *J. Mech. Phys. Solids* **41,** 1357–1382.

Rashid, M. M. (1992). Texture evolution and plastic response of two-dimensional polycrystals. *J. Mech. Phys. Solids* **40,** 1009–1029.

Rice, J. R. (1971). Inelastic constitutive relations for solids: an internal-variable theory and its application to mental plasticity. *J. Mech. Phys. Solids* **19,** 433–455.

Stout, M. G. and O'Rourke, J. A. (1989). Experimental deformation textures of OFE copper and 70:30 brass from wire drawing, compression, and torsion. *Metall. Trans.* **20A,** 125–131.

Toth, L. S., Gilormini, P. and Jonas, J. J. (1988). Effect of rate sensitivity on the stability of torsion textures. *Acta Metall.* **36,** 3077–3091.

Toth, L. S., Neale, K. W. and Jonas, J. J. (1989). Stress response and persistence characteristics of the ideal orientations of shear textures. *Acta Metall.* **37,** 2197–2210.

Toth, L. S., Jonas, J. J., Gilormini, P. and Barcroix, B. (1990). Length changes during free-end torsion: a rate sensitive analysis. *Int. J. Plasticity* **6,** 83–108.

Toth, L. S., Jonas, J. J., Daniel, D. and Bailey, J. A. (1992). Texture development and length changes in copper bars subjected to free-end torsion. *Text. Microstruct.* **19,** 245–262.

Van Der Giessen, E. (1989). On a continuum representation of deformation-induced anistropy. In *Advances in Constitutive Laws for Engineering Materials* (eds J. Fan and S. Murakami), pp. 503–509, Pergamon Press, Beijing.

Van Der Giessen, E. (1991). Micromechanical and thermodynamic aspects of the plastic spin. *Int. J. Plasticity* **7,** 365–386.

Van Der Giessen, E. and Van Houtte, P. (1992). A 2D analytical multiple slip model for continuum texture development and plastic spin. *Mech. Mater.* **13,** 93–115.

Wang, P. T., Panchanadeeswaran, S. and Wu, H. C. (1995). Comparison of flow stress and texture for P0818 cast aluminum deformed in compression and in torsion. Alcoa Technical Center Research Report, Alcoa Center, Pennsylvania, U.S.A.

White, C. S. (1992). An analysis of the thin-walled torsion specimen. *ASME Trans., J. Engng Mat. Tech.* **114,** 384–389.

Wu, H. C., Xu, Z. Y. and Wang, P. T. (1992). The shear stress strain curve determination from torsion test in the large strain range. *ASTM J. Test. Eval.* **20,** 396–402.

Wu, H. C., Xu, Z. Y. and Wang, P. T. (1993). An experimental investigation of torsion at room and elevated temperatures in the large strain range. In *4th Int. Symp. Plasticity and Its Current Applications*, Baltimore, MD, 19–23 July, 1993.

Wu, H. C., Xu, Z. Y. and Wang, P. T. (1995a). Determination of shear stress–strain curve from torsion tests for loading–unloading and cyclic loading. Research Report SMT-95-1, submitted to Alcoa Technical Center, Department of Civil and Environmental Engineering, The University of Iowa.

Wu, H. C., Xu, Z. Y. and Wang, P. T. (1995b). Torsion testing of aluminum in the large strain range. Research Report SMT-95-2, submitted to Alcoa Technical Center, Department of Civil and Environmental Engineering, The University of Iowa.